Stochastic resonance in mammalian neuronal networks

Bruce J. Gluckman[a] and Paul So
Department of Physics and Astronomy and The Krasnow Institute for Advanced Studies, George Mason University, Fairfax, Virginia 22030

Theoden I. Netoff
Program in Neuroscience, The George Washington University, Washington, DC 20052

Mark L. Spano
Naval Surface Warfare Center, Carterock Division, West Bethesda, Maryland 20817

Steven J. Schiff
The Krasnow Institute for Advanced Studies and the Department of Psychology, George Mason University, Fairfax, Virginia 22030 and Program in Neuroscience, The George Washington University, Washington, DC 20052

(Received 26 February 1998; accepted for publication 25 May 1998)

We present stochastic resonance observed in the dynamics of neuronal networks from mammalian brain. Both sinusoidal signals and random noise were superimposed into an applied electric field. As the amplitude of the noise component was increased, an optimization (increase then decrease) in the signal-to-noise ratio of the network response to the sinusoidal signal was observed. The relationship between the measures used to characterize the dynamics is discussed. Finally, a computational model of these neuronal networks that includes the neuronal interactions with the electric field is presented to illustrate the physics behind the essential features of the experiment. © *1998 American Institute of Physics.* [S1054-1500(98)01703-0]

Biological systems, brains especially, are replete with noise: membrane channels open and close randomly, quantal release at synapses is probabilistic, thermal and ionic regulation is imperfect, a neuron's extracellular field potential fluctuates with both nearby and distant neighbors' firing, and action potentials often appear to occur stochastically. The conjecture that noise is utilized in neuronal computation is not new,[1] yet the new developments in the physics of noise interaction with nonlinear systems throw a fresh perspective on this topic. Stochastic resonance (SR), an effect in which the addition of noise enhances a system's response to small signals,[2–4] has been suggested as a mechanism for noise to play a positive role in neuronal information processing.[5,6] SR has been shown in the conductance of ion channels in membranes,[7–9] in theoretical models of neurons[10–15] and models of neuronal arrays,[16–18] and demonstrated experimentally for sensory processes in crayfish,[19–21] crickets,[22] rat skin,[23] human muscle spindles[24] and tactile sensation,[25] and even the psychophysics of human vision.[26] We report here the details of the first demonstration of SR in a live neuronal network from mammalian brain,[27] in which both signal and noise were presented to the network via an imposed electric field.[28] Results from a model network of excitatory neurons from this network are provided to clarify the underlying physics of this experimental system.

I. INTRODUCTION

Stochastic resonance was initially introduced to explain why the observed periodicity of the ice ages matched the periodicity of small fluctuations in the earth's orbit.[29] Since its introduction, SR has been observed in numerous physical systems.[2–4] Similarities between distributions of interevent intervals in systems demonstrating SR and interspike interval histograms (ISIH) indicated that SR might play a role in neuronal dynamics,[5,6] and SR was shown in theoretical models of single neurons,[10,12–15] and models of neuronal networks.[16–18] Experimentally, neuronal SR has been demonstrated in the activities of single mechanoreceptive sensory neurons from crayfish[19,20] and rat skin,[16] and of interneurons from the cricket abdominal ganglia.[22] In addition, SR has been reported in human muscle-spindle receptors[24] and human tactile sensation.[25] In each of these demonstrations, SR involved the processing of mechanosensory information in which both signal and noise were encoded into environmental pressure fluctuations. In Ref. 21, detection of pressure fluctuation signals in the crayfish tailfan ganglia was shown to be enhanced by the noisy output of caudal photoreceptors. SR has also been reported in perceptual tasks in human vision,[26] in which spatially and temporally varying noise was added to a static pattern; the minimum amplitude needed to resolve an aspect of the pattern was optimized at moderate

[a]To whom correspondence should be addressed; Electronic mail: BGluckma@GMU.edu

noise levels. Our objective in the present work was to demonstrate SR in neurons from mammalian brain. The key technical problem to overcome was the need to directly modulate the noise felt by the neurons.[4]

In the broadest definition, SR occurs when the addition of noise to a system enhances its response to an otherwise subthreshold signal, with an optimum response occurring at finite noise level. Several approaches to the definition of ''optimal response'' have been used. In the classical SR paradigm, optimization is characterized by the ability to detect the presence of a subthreshold periodic signal. In this case, optimization is defined as a maximum in the signal to noise ratio (SNR), defined from the power spectrum, at a finite noise level. Under this criteria, what is optimized is detection of the frequency of the signal, not detection of its amplitude or phase. An alternate formulation for SR involves a matching or coincidence between the time scale of the noise driven dynamics and the period of the subthreshold signal, making it a true resonance.[30] Maximal SNR is then accompanied by maximal height or area of particular peaks in the normalized ISIH as a function of noise amplitude.

Detection optimization for aperiodic signals has also been shown. In this aperiodic SR (ASR), measures of correlation[23,31] and mutual information[22,32] between the input and output were optimized at finite noise level. In a recent paper, Eichwald and Walleczek[33] showed that ASR can also involve matching of time scales between the noise driven dynamics and the signal.

Each of the above optimized statistical measures imply long time averages of the system response in order to determine the signal. Averaging can also be achieved by summing over the outputs of an ensemble of dynamical units receiving the signal, each with its own independent noise signal. As the size of the ensemble is increased, optimization of the correlation between input and output becomes independent of signal frequency and noise amplitude, provided the noise amplitude is above a minimum level.[34] Recently, a number of authors have approached the question of optimization in terms of information transfer.[22,23,35,36] Notably, Stemmler[35] has shown theoretically that three different measures are optimized as a function of input noise in leaky integrate and fire model neurons: the probability of correctly estimating a constant input in a short time, the SNR in response to a sinusoidal input, and the mutual information between an arbitrary input signal and the output spike train.

In this work we demonstrate classical periodically driven SR in a live neuronal network from rat hippocampus.[27] We apply both signal and noise via an imposed electric field,[28] and measure the response of the network in the form of synchronous burst firing events. We find an optimization in the SNR which occurs at finite noise level. In addition, we find that optimization occurs approximately at a matching between noise driven dynamics and the period of the drive. We then clarify and support these results with a computational model.

II. EXPERIMENTAL METHODS

Hippocampal slices were prepared from 125 to 150 g Sprague-Dawley rats, which were deeply anesthetized in diethyl-ether and decapitated. Slices were cut either transversely or longitudinally with respect to the long axis of the hippocampus using a tissue chopper, and placed in an interface type perfusion chamber at 34 °C–36 °C. Slices were perfused with an artificial cerebrospinal fluid (ACSF) composed of (in mM) 155 mM Na^+, 136 mM Cl^-, 3.5 mM K^+, 1.2 mM Ca^{2+}, 1.2 mM Mg^{2+}, 1.25 mM PO_4^{2-}, 24 mM HCO_3^-, 1.2 mM SO_4^{2-}, and 10 mM dextrose, flowing at 2 ml/min. After 90 min, the ACSF was switched to one containing 8.5 mM KCl, the other ionic constituents remaining the same.

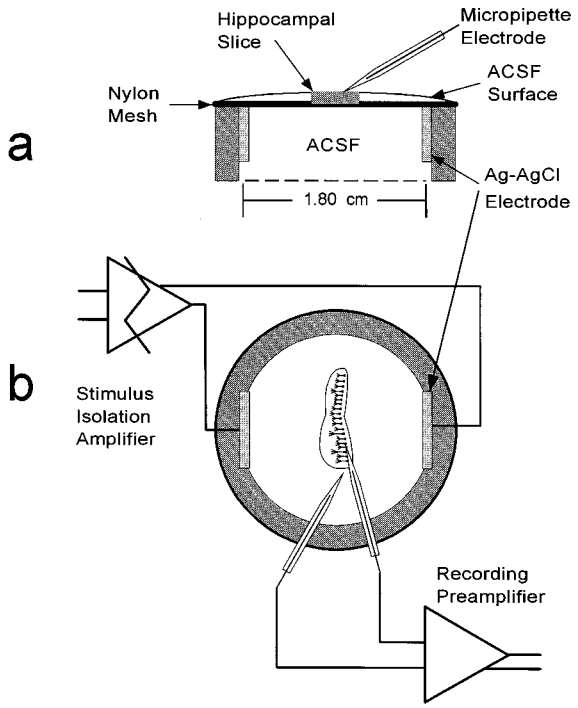

FIG. 1. Schematic of perfusion chamber as viewed from (a) the side and (b) the top. The hippocampal slice rests on a nylon mesh just below the surface of the perfusate. An electric field is applied to the slices by applying a potential difference through an isolation amplifier between two parallel plate Ag–AgCl electrodes submersed in the bath [after Ref. 28, Figs. 1(a) and 1(b)].

A perfusion chamber was designed so that a spatially uniform electric field could be applied to these networks. This was accomplished by installing a pair of parallel plate nonpolarizing electrodes (Ag–AgCl) submerged in the bath, as illustrated schematically in Fig. 1. The electric field was then imposed by applying a potential difference between the electrodes through an isolation amplifier.

The electric field in the chamber was measured and mapped both with and without a slice present, as shown in Fig. 2. Since these electrodes slowly polarize with constant applied current, these mappings were done by applying an ac field and measuring the root-mean-square (rms) amplitude and phase of the response. No significant frequency dependence was observed between 5 and 65 Hz [Fig. 2(b) lower inset], nor were significant differences observed between the field in the slice and in the bath with the slice removed [Fig. 2(b) upper inset]. These measurements were made 50 mm from the surface of the slice; similar results were found at a depth of 100 mm (not shown). The field within the slice was

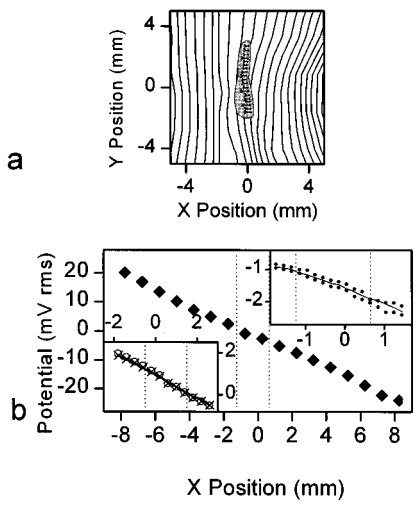

FIG. 2. Mappings of the electric field in the chamber, measured by applying a sinusoidal potential with frequency f_0 and measuring locally the phase and power of the potential with respect to a fixed point in the chamber ($f_0 = 60$ Hz unless otherwise specified). (a) Spatially resolved isopotential lines over the central 1 cm^2 area of the chamber, where the slices sit. (b) Potential within the chamber with and without a slice present as a function of transverse position, X. Main graph: Potential averaged over $-3<Y<3$ mm. Upper inset: Potential ● with slice and — without slice. Lower inset: Potential ○ with slice ($f=65$ Hz), × with slice ($f=5\,Hz$), and — without slice ($f=35$ Hz) [after Ref. 28, Figs. 1(c) and 1(d)].

fairly uniform, nearly identical to the field within the chamber, and proportional to the applied potential for the range of frequencies used in this experiment.

When perfused at an elevated potassium level (8.5mM rather than the normal 3.5 mM [K^+]), these networks exhibit spontaneous synchronous activity in which large populations of the main excitatory neurons (pyramidal cells) fire synchronously in bursts. Such activity is an emergent property of the network, and is observed as large stereotyped extracellular potential changes in the cell body layers (CA1 or CA3 regions of the hippocampus[37]). We recorded such dynamics using paired saline-filled micropipettes (1–4 MΩ) and a differential dc-coupled preamplifier (Grass Model P16). These signals were then fed to an analog to digital converter in a computer and stored. In order to subtract the applied field from the recording, we aligned the two electrodes as close to the same isopotential of the field as possible, one within and one external to the slice. After placing the recording electrode in the pyramidal cell body layer, the reference electrode position was adjusted to minimize the signature of a small applied 10 Hz sinusoidal field. Following this electrode placement, continuous recordings of neuronal activity could be performed during application of relatively substantial electric fields.

Unfortunately, some residual stimulus artifact often remained in the recorded signal. For this reason, we chose applied signals which could be discriminated from the neuronal dynamics based on frequency. Bursts typically last 10–30 ms, occur as frequently as a few Hz, and can be identified from characteristic frequency components near 250 Hz. We therefore chose input signals containing frequencies lower than this burst signature. Sinusoids were selected with frequencies $f_0<4$ Hz, and superimposed with random fluctuations (noise) with high frequency cutoff f_N such that $f_0 \ll f_N \ll 250$ Hz.

In order to further minimize leakage of stimulus into the measurement statistics, we extracted from the recordings only the onset times $\{t_n\}$ of the synchronous network bursts. We thereby also ignore the asynchronous neuronal activity. This practice is in agreement with classical SR, in which a system's subthreshold activity is ignored and only superthreshold events are considered. Bursts were detected by first processing the recorded signal to sample the local power within a frequency band around 250 Hz, then finding threshold crossings that reliably discriminated these events. Statistical measures such as the burst rate and power spectral density (PSD) were then derived from these event time series.

The PSDs were approximated from the event series $\{t_n\}$ in the following manner. We constructed a continuous time series $Y(t)$ by placing a structure function $S(t)$, chosen to have finite area, at each event time, $Y(t)=\Sigma_n S(t-t_n)$. The Fourier transform of $Y(t)$ is then

$$\tilde{Y}(\omega)=\int e^{-i\omega t}\sum_n S(t-t_n)\,dt=\sum_n e^{-i\omega t_n}\tilde{S}(\omega), \qquad (1)$$

where $\tilde{S}(\omega)$ is the Fourier transform of $S(t)$. For simplicity, we chose a Dirac delta function for $S(t)=\delta(t)$, although we have also used Gaussian functions having widths proportional to the event durations with comparable results. The structure function choice affects primarily the high frequency components of the spectrum, with which we are not concerned. The Fourier transform then reduces to

$$\tilde{Y}(\omega)=\int e^{-i\omega t}\sum_n \delta(t-t_n)\,dt=\sum_n e^{-i\omega t_n}, \qquad (2)$$

and the PSD is then computed in the normal way, $\mathrm{PSD}(\omega)=\tilde{Y}(\omega)\tilde{Y}^*(\omega)/T$, where * denotes complex conjugate and T is the actual time over which the data was measured. As with other methods of approximating PSDs from finite time series,[38] this method is limited to evaluation at frequencies that are integer mutiples of T^{-1} (i.e., $\omega=n2\pi/T$). Since this formulation deals only with point processes, there is no *a priori* high frequency cutoff.

Waveforms were computer generated at 10 kHz using a digital to analog (DA) converter (National Instruments AT-MIO16X), then low pass filtered at 3 kHz to remove high frequency DA conversion artifacts. This provided sufficient fidelity for the signals used, whose frequency content were well below 250 Hz. A finite bandwidth noise function was formed by extrapolating between values chosen at equal time intervals from a Gaussian distributed random distribution. The extrapolation was done using a fourth order polynomial, which ensured that both the signal and its derivative were continuous. An example of this noise function is shown in Fig. 3(a) at high resolution with vertical grid lines at the update times $t_n=n/(2f_N)$, and shown at a compressed time base in the inset. This noise function is delta correlated for times greater than the update time [Fig. 3(b)], and, as expected, its frequency spectrum decays rapidly for frequencies above f_N [Fig. 3(c)].

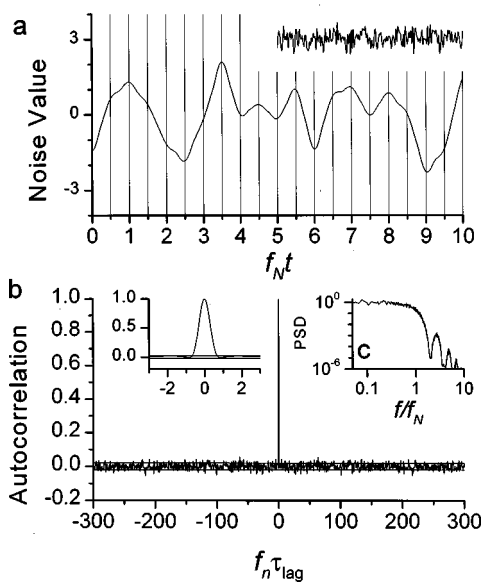

FIG. 3. Specifics of the noise function used in both experiments and computations. (a) Waveform at high resolution showing randomly chosen deviations at half multiples of the noise period with smooth interpolation and (inset) long term behavior (100 cycles). (b) Autocorrelation function of noise function, which is delta correlated for time lags greater than the update time $t_n = n/2f_N$ (though smooth and correlated for shorter lags) (inset). (c) Power spectral density of the noise function.

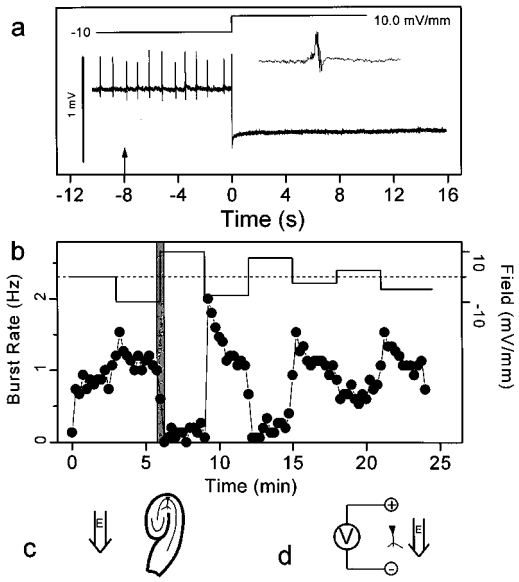

FIG. 4. Suppression or enhancement of spontaneous synchronous neuronal activity (bursts) by a constant applied electric field. (a) Trace of measured field potential (main trace) from the CA3 region of a transverse slice as a function of time during applied field (upper trace). Detail of a single burst shown in the inset at an expanded time base (0.5 s long, arbitrary vertical scale, origin marked by ↑ in the main figure.). (b) Mean burst rate (connected dots), calculated within 15s windows, under the influence of applied electric field (solid line). Without applied field, pyramidal cells synchronously discharge at ~1 Hz. Negative field amplitudes accelerate whereas positive amplitudes suppress burst rate. The shaded region corresponds to the time in (a). (c) Orientation of slice with respect to the applied field. (d) Orientation and polarity of the applied field with respect to the axis defined from the soma to apical dendrites of the main excitatory neurons (after Ref. 28, Figs. 3, 4).

III. EXPERIMENTAL RESULTS

The effects of electric field changes on spontaneous activity are illustrated in Fig. 4(a) for transversely cut slices, measured from the CA3 region. The applied electric field is indicated by the upper trace. Details of a single burst (the one indicated by the ↑), with its characteristic 250 Hz frequency signature, is shown in the inset at an expanded time base. With the application of a moderate field, 10 mV/mm, we have significantly modulated the spontaneous activity and literally turned off the synchronous bursts. However, the effect is actually graded over a range of field amplitudes. This can be seen from the mean burst rate a function of the applied dc field amplitude, shown in Fig. 4(b) for the same network. Here, the mean burst rate, computed for 15 s time windows, increases or decreases from its resting value of 0.8 Hz as graded amounts of negative or positive field were applied. Our notation for the sign of the field with respect to the soma and apical dendrites of the pyramidal cell layer in this network is indicated by the diagram in Fig. 4(c). Similar modulatory effects can be observed in both CA3 and CA1 layers whether transversely or longitudinally cut, provided the field is aligned parallel to the somatic-dendritic axis of the primary pyramidal neurons of the layer as indicated in Fig. 4(d). For further details, see Ref. 28.

To demonstrate SR, we utilized this electric field interaction to supply both signal and noise to neuronal networks. In the simplest example (Fig. 5), we chose networks which were not spontaneously bursting, though bursts could be excited with either a dc field or a sinusoidal field with amplitude A_S above some nonzero threshold, A_{ST}. If we applied a noise signal with amplitude A_N to such a slice, we observed randomly occurring bursts. When we applied a combination of this noise and a subthreshold sinusoid ($A_S < A_{ST}$), random bursts were observed, but clustered preferentially within a restricted phase of the sinusoid. Typical responses of the network to a field with only a subthreshold sinusoid, only noise, and a combination of both are shown in Fig. 5. In each panel of Fig. 5, the upper trace is the recorded signal filtered (band pass, rectified, and smoothed) to indicate the locations of the network bursts, which appear as large peaks. Note that small deviations in this trace, such as seen in Fig. 5(a), are reflective of an increased level of asynchronous neuronal excitation but not reflective of synchronous network bursts. The difference can be observed by comparing the traces of the raw extracellular measurements shown in the insets of Figs. 5(a) and 5(b). The activity in Fig. 5(b) is a burst. The middle and lower traces are respectively the sinusoidal and noise components of the applied field.

It is instructive to look at the response of the system in terms of the phase of the subthreshold sinusoid. For this, we introduce the burst probability density as a function of the phase (BPDP) of the drive, $P_\phi(\phi) = (\tau/T)\Sigma_n \delta(\phi - \phi_n)$, where $\phi_n = \mathrm{mod}\,(t_n, \tau)$ is the phase of the nth event with respect to the sinusoid and has units of time, $\tau = 1/f_0$ is the period of the drive [see Fig. 6(a)], and T is the total measurement time. This measure is analogous in the neurophysiology literature to the normalized post- or peri-stimulus time histogram.[39] Note that we have normalized this probability

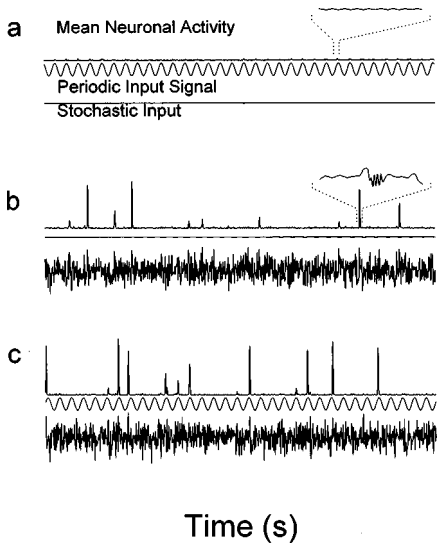

FIG. 5. Activity in CA1 layer of a longitudinal slice with an imposed electric field. In each panel, the upper trace is the recorded field potential filtered (band passed between 200–1000 Hz, then rectified and smoothed) to indicate timings of bursts. The lower two traces are, respectively, the periodic and stochastic components of the applied field. In order to highlight the phase coherence between the signal and the neuronal response, negative field is plotted as an *upward* deflection. (a) With just the subthreshold sinusoid, no bursts are observed ($f_0=3.3$ Hz, $A_s=3.75$ mV/mm). (b) With just noise, bursts occur randomly ($f_N=26$ Hz, $A_N=10$ mV/mm). (c) With both subthreshold sinusoid and noise, bursts occur randomly, but preferentially near the peaks of the sinusoid (negative field). The insets in (a) and (b) are short (0.14 s) traces of the raw extracellular field potential [modified from Ref. 28, Fig. 2, © 1997 by the American Physical Society (APS)].

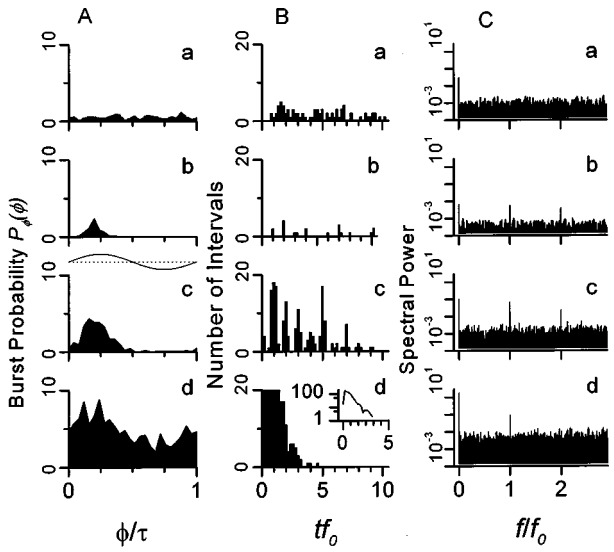

FIG. 6. (a) Burst probabiltiy density as a function of phase (BPDP), $P_\phi(\phi)$, (b) interspike interval histogram (ISIH), and (c) power spectral density (PSD) from the same experiment as in Fig. 5 ($f_0=3.3$ Hz, $f_N=26$ Hz). The field amplitudes (in mV/mm), signal to noise ratio (SNR), and the mean burst rate per drive cycle, $r_e\tau$, are given in the table below (modified from Ref. 28, Fig. 3, © 1997 APS).

Statistics for graphs in Fig. 6.

row	A_s (mV/mm)	A_N (mV/mm)	SNR	$r_e\tau$
a	0.00	10	0	0.16 ± 0.01
b	3.75	5	18	0.08 ± 0.01
c	3.75	10	82	0.31 ± 0.02
d	3.75	20	29	1.35 ± 0.05

such that its integral is equal to the average number of events per cycle of the drive, i.e., $\int_0^\tau P_\phi(\phi)\, d\phi = r_e\tau$, where r_e is the mean event rate. If this were a simple static (history-free) threshold system, the BPDP would be a direct measure of the probability that the sum of the noise and signal were over threshold as a function of the phase of the sinusoid.

The BPDP is shown in the first column of Fig. 6 for various combinations of signal and noise. In the top row, with moderate noise and no subthreshold sinusoid, no phase dependence is observed. With small noise and a subthreshold sinusoid (second row), this function displays a small peak. Then, as a function of increasing noise amplitude, the peak grows and widens (third and fourth rows). The field settings for these plots are listed in the table in the legend of Fig. 6, along with the mean burst rate per drive cycle, $r_e\tau$, and the signal to noise ratio (SNR), to be discussed below.

Neurophysiological data is often analyzed using the interspike (or interevent) interval histogram (ISIH),[39] and neuronal SR has been inferred from periodic modulation observed in ISIHs.[5,6] The ISIHs for this same experiment are shown in the middle column of Fig. 6. Without a sinusoidal signal [Fig. 6(a)], the ISIH is featureless. With both the sinusoid and a small amount of noise [Fig. 6(b)], the ISIH appears with peaks at integer multiples of the drive period. As the noise amplitude is then increased [Figs. 6(c) and 6(d)], these peaks increase in width, and the envelope describing their height appears more exponential [inset in Fig. 6(d)], with the decay time of the exponential decreasing with increasing noise. In the next section, we show the relationship between this decay rate and the mean event rate, which in turn is an increasing function of noise. Note that at the highest noise level shown (bottom row), with the highest mean burst rate, modulation by the sinusoid can still clearly be seen in the BPDP, although separate peaks are no longer distinguishable within the ISIH.

If we now look at the power spectral density (PSD) as a function of frequency for the same settings, shown in the right column in Fig. 6, we find that without an applied sinusoidal signal, the response is spectrally white. With a combination of subthreshold sinusoid and small noise, peaks appear at integer multiples of the sinusoidal drive frequency f_0 on top of a white background. As the noise level in the input is increased, the amplitudes of both the peak at f_0 and of the background increase.

SR is typically phrased in terms of signal transmission, or how well the subthreshold signal can be detected from the observed dynamics. This is typically characterized by the SNR defined from the PSD as the ratio of the power at f_0 to the background (bkg), presented in decibels, $\mathrm{SNR}=10\log_{10}(\mathrm{PSD}(f_0)/\mathrm{PSD}(\mathrm{bkg}))$. In these experiments, the SNR is maximal at an intermediate level of input noise. The SNR as a function of noise intensity, A_N, with constant si-

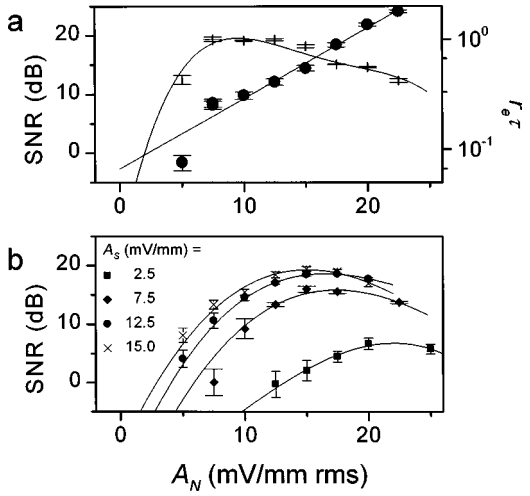

FIG. 7. Signal to noise ratio (SNR) in decibels [$10\log_{10}$(SNR)] as a function of A_N (a) for the experiment in Figs. 5 and 6 ($f_0=3.3$ Hz, $f_N=26$ Hz), and (b) a different experiment ($f_0=3.09$ Hz, $f_N=20$ Hz). In both cases, no bursts were observed for $A_N=0$, so SNR(0)=0. Solid lines are provided to guide the eye. Error bars are estimated from the variance between multiple measurements where possible, or proportional to counting error (inverse square root of the number of intervals) (modified from Ref. 27, Fig. 4, © 1997 APS).

nusoid amplitude, A_S, is shown in Fig. 7(a) (bars) for the same experiment as in Figs. 5 and 6. In addition, we have plotted [Fig. 7(a), filled circles] the mean bursts per cycle of the drive, $r_e\tau$, which increases monotonically with A_N. We note that the SNR is maximum when $r_e\tau\sim 0.4$ (0.4 spikes per period of the drive).

A series of optimization curves for various values of A_S is shown in Fig. 7(b) from a different experiment. As A_S is increased toward the threshold, the maximal value for the SNR increases and occurs at lower A_N. Experiments were performed on 12 slices from nine rats. When analyzed as in Fig. 7, SR was documented in nine experiments from the CA1 (five longitudinally and two transversely cut slices) and CA3 layers (two transverse slices).

In some of the experiments performed, the slice was spontaneously active without any applied field. In these cases, a finite SNR was observed with no applied noise. Nevertheless, an increase in and optimization of SNR was found with the addition of noise to the input signal.

IV. RELATION BETWEEN MEASURES

For point process or event time data, as in this experiment, the three measures presented, BPDP, ISIH and PSD, are related to each other. The power spectrum and the BPDP are intimately related because the Fourier transform of the delta function time series at $f_0=1/\tau$ is proportional to an integral over the BPDP, $\tilde{Y}(\omega_0=2\pi/\tau)\propto\int e^{-i\omega_0\phi}P_\phi(\phi)\,d\phi$. This is seen by substituting $\omega_0=2\pi/\tau$ into (2):

$$\tilde{Y}(\omega_0)=\sum_n e^{-i\omega_0 t_n}=\sum_n e^{-i\omega_0\phi_n}.$$

The latter step follows from the fact that each ϕ_n and t_n differ by an integer multiple, l_n, of τ, i.e., $\phi_n=t_n+l_n\tau$, and $e^{i\omega_0 l_n\tau}=1$. We then insert $1=\int_0^\tau\delta(\phi-\phi_n)\,d\phi$ into the above equation:

$$\begin{aligned}\tilde{Y}(\omega_0)&=\sum_n\int_0^\tau\delta(\phi-\phi_n)\,d\phi e^{-i\omega_0\phi_n}\\&=\int_0^\tau e^{-i\omega_0\phi}\sum_n\delta(\phi-\phi_n)\,d\phi\\&=\frac{T}{\tau}\int_0^\tau e^{-i\omega_0\phi}P_\phi(\phi)\,d\phi.\end{aligned}$$

If a structure function other than $\delta(t)$ is used, this result is modified to

$$\tilde{Y}(\omega_0)\propto\tilde{S}(\omega_0)\int_0^\tau e^{-i\omega_0\phi}P_\phi(\phi)\,d\phi.$$

The ISIH is also related to the PSD. Specifically, it is a term in a series expansion of the autocorrelation function $G(\Delta)$ (the Fourier transform of the PSD), where Δ is a lag time. This can be seen directly by substituting the delta-function series approximation for the time series $Y(t)=\Sigma_m\delta(t-t_m)$ into the definition of $G(\Delta)$ as follows:

$$\begin{aligned}G(\Delta)&\equiv K\int Y(t)Y(t-\Delta)dt\\&=K\int\sum_m\delta(t-t_m)\sum_n\delta(t-t_n-\Delta)\,dt\\&=K\sum_m\sum_n\delta(t_m-t_n\Delta),\end{aligned}$$

where K is the standard normalization, $K^{-1}=\int Y^2(t)\,dt$. If we now adopt the notation I_m^j for the interval between events m and $m-j$, $I_m^j=t_m-t_{m-j}$, where $j=m-n$, then the above equation reduces to

$$G(\Delta)=K\sum_j\sum_m\delta(I_m^j-\Delta)\propto\sum_j P_{ISI(j)}(\Delta),\tag{3}$$

where $P_{ISI(j)}(I)=(1/M)\,\Sigma_m\delta(I_m^j I)$ is the jth passage probability density (M is the total number of events counted). $P_{ISI(j)}(I)$ for $j=1$ is the normalized ISIH, where the normalization is such that $\int P_{ISI(j)}(I)\,dI=1$. Note that the above analysis applies in the limit of infinite data. Numerical estimation of probability density functions from finite point process data has recently been discussed in Ref. 40. In addition, we note that if one chooses a structure function other than $\delta(t)$ in, then the above result is

$$G(\Delta)\propto\sum_j\int S_2(I'-\Delta)P_{ISI(j)}(I')\,dI',$$

where $S_2(\Delta)=\int S(t)S(t-\Delta)\,dt$ is the convolution of the structure function with itself.

The normalized ISIH can also be directly related to the BPDP, provided the refractory (or relaxation) time for the dynamics is sufficiently short with respect to the period of

the sinusoid as to be negligible. In this case, the BPDP is equal to the instantaneous probability density of an event occurring, and $P_{ISI(1)}(I)$ can be written

$$P_{ISI(1)}(I)=\frac{1}{r_e\tau}\int_0^{\tau}P_{\phi}(\phi_0)P_{\phi}(\phi_0+I)\times e^{-\int_0^I P_{\phi}(\phi_0+t)\,dt}\,d\phi_0. \quad (4)$$

This relation can be derived as follows. We first consider the distribution of events $P_{ISI(1)}(I,\phi_0)$ following an event observed at a particular phase ϕ_0. We next introduce the probability $R(I,\phi_0)$ that a second event has not been observed after an interval I following this initial event. The probability density of actually observing the next event at time ϕ_0+I is the product of $R(I,\phi_0)$ with the probability density of seeing an event at that time, i.e., $R(I,\phi_0)P_{\phi}(\phi_0+I)$. The total interevent interval probability density, $P_{ISI(1)}(I)$, is the ensemble average of this joint probability density over all initial phases ϕ_0.

$$P_{ISI(1)}(I)=\frac{\int_0^{\tau}P_{\phi}(\phi_0)(R(I,\phi_0)P_{\phi}(\phi_0+I))\,d\phi_0}{\int_0^{\tau}P_{\phi}(\phi_0)\,d\phi_0}. \quad (5)$$

To complete this description, we obtain an expression for $R(I,\phi_0)$ as follows. The differential decrease in $R(I,\phi_0)$ within an interval dI is equal to the probability that a new event has been observed within the interval $[\phi_0+I,\phi_0+I+dI]$, equal to $R(I,\phi_0)P_{\phi}(\phi_0+I)\,dI$. Therefore,

$$dR(I,\phi_0)=-R(I,\phi_0)P_{\phi}(\phi_0+I)dI.$$

This equation has a solution $R(I,\phi_0)=e^{-\int_0^I P_{\phi}(\phi_0+t)dt}$. By inserting this result into (5), one obtains equation Eq. (4). We note that (4) was presented for escape-time distributions from a two-well potential.[41]

By assuming that the refractory time was small with respect to the drive period, we could interpret $P_{\phi}(\phi)$ as a measure of the instantaneous probability density that the signal plus noise is above the rest-state threshold as a function of stimulus phase. Note that when the refractory period is not negligible when compared to the drive period, this approximation is no longer valid; in this case, $P_{\phi}(\phi)$ will differ from the probability that the signal plus noise is above the rest state threshold, and $P_{\phi}(\phi)$ can have a maximum at a different phase.

It is useful to consider the behavior of (4) at integer multiples of the drive period, $I=n\tau$. In this case, the exponentiated integral reduces to $\int_0^{n\tau}P_{\phi}(\phi_0+t)\,dt=nr_e\tau$, i.e., n times the mean number of bursts per cycle of the drive. In addition, $P_{\phi}(\phi_0+n\tau)=P_{\phi}(\phi_0)$, so (4) can be written in the reduced form

$$P_{ISI(1)}(n\tau)=\frac{e^{-nr_e\tau}}{r_e\tau}\int_0^{2\pi}P_{\phi}(\phi_0)P_{\phi}(\phi_0)\,d\phi_0.$$

Using the same considerations, one also finds the general result

$$P_{ISI(1)}(n\tau+\phi)=e^{-nr_e\tau}P_{ISI(1)}(\phi). \quad (6)$$

This confirms the important result that the envelope function of this ISIH has an exponential dependence with a decay rate equal to the mean event rate, r_e. This is the same decay rate expected for the ISIH of an unmodulated renewal process.[39] Most importantly, one can use the self-similar relation (6) and the normalization of $P_{ISI(1)}(I)$ to argue that each peak at $n\tau$ in the ISIH, or the area under each peak, is maximal at finite $r_e\tau$. For example, the area P_n under the ISIH in the interval $[n\tau,n\tau+\tau]$ is

$$P_n=P_0e^{-nr_e\tau}=(1-e^{-r_e\tau})e^{-nr_e\tau}. \quad (7)$$

This area, P_n, has a maximum as a function of the mean rate r_e at $r_e\tau=-\ln(n/n+1)$, for $n>0$. Since we expect that the mean event rate should increase as we increase the noise level, this provides insight into why a particular peak in the ISIH should optimize at finite noise level.

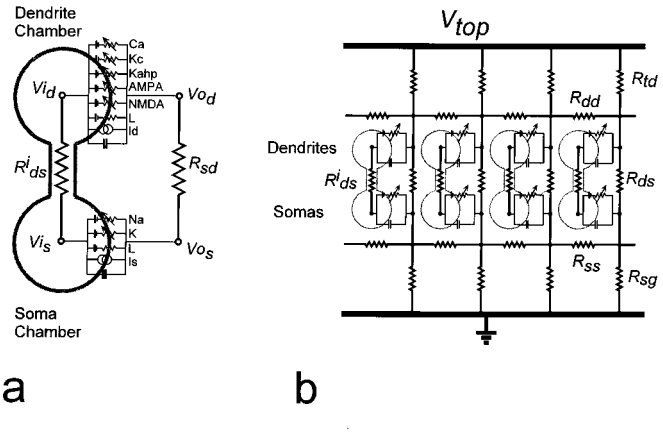

FIG. 8. Schematic of two-chamber model for CA3 pyramidal neurons incorporating electric field effects. (a) Detailed circuit diagram for a single neuron, including two active conductances in the soma chamber and five in the dendrite chamber, plus capacitance and passive leakage conductances in each. Symbols as in the text. (b) Circuit diagram of a linear array of neurons. An electric field is applied by imposing a potential difference between the upper and lower isopotentials.

V. COMPUTATIONAL MODEL

In order to illustrate the physics of these experiments, we have built a computational model of a network of the main excitatory neurons from the hippocampal CA3 region. The model is based on Pinsky and Rinzel's[42] two-chamber lumped parameter reduced version of Traub *et al.*'s[43] 19-compartment cable model of CA3 pyramidal neurons. In the model, each neuron is envisioned to have two chambers, one characterizing the soma, where action potentials are initiated, and one for the dendrites, as illustrated in Fig. 8(a). The two chambers are electrically coupled by a finite resistance, R_{sd}^i, and are coupled to the extracellular space both capacitively and by parallel voltage dependent variable resistors, each in series with a voltage source to model active ionic channels and concentration gradients. In addition, each chamber has a passive leakage resistance (L), and can have an additional current injected into it (*Is* and *Id*). A main advantage of the reduced model is its computational efficiency, as these simulations are run on desktop PCs.

The soma chamber has two kinds of voltage dependent resistors, to model sodium (Na) and potassium (K) channels. The dendrite chamber has five active resistances: for calcium

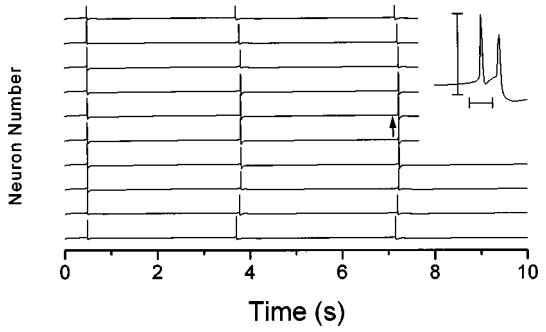

FIG. 9. Traces of somatic transmembrane potential as a function of time for an array of ten coupled model neurons. The neurons fire in synchronous bursts. Inset: Details of a single neuron's firing (a spike doublet whose position is marked by the arrow in the main graph) at an expanded time scale. The vertical and horizontal scale bars correspond to 100 mV and 10 ms.

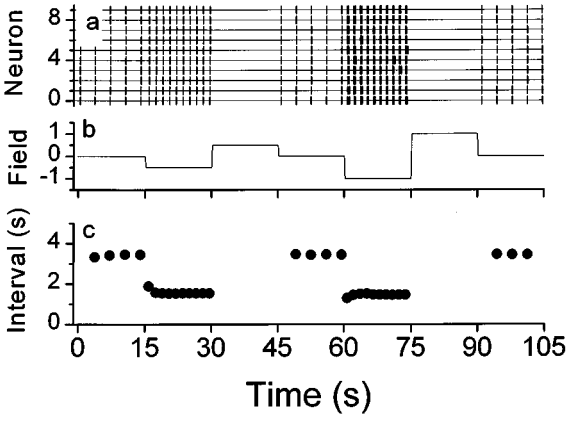

FIG. 10. Response of a network of ten neurons under the influence of a dc field. (a) Onset times of spikes (|) as a function of time and neuron number. (b) Applied field, in units of (mV/dendritic-somatic distance). (c) Interval between network bursts as a function of time.

(Ca), calcium dependent potassium (Kc), potassium after hyperpolarization (Kahp), and for DL-alpha-amino-3-hydroxy-5-methylisoxazole-propionic acid (AMPA) and N-methyl D-aspartate (NMDA) mediated synaptic currents.

As originally conceived,[42] the reduced pyramidal cell model had no spatial extent. In order to couple in the electric field, we allow the extracellular potential outside the dendritic chamber to differ from that outside the somatic chamber, separating them with a finite extracellular resistance, R_{ds}. A network of these individual neurons is assembled into a linear resistive array as illustrated in Fig. 8(b). In addition to the resistive coupling, the neurons are synaptically coupled to their four nearest neighbors on each side (not shown). An electric field is now applied to this network by making the potential of the upper isopotential, V_{top} different from the potential of the lower isopotential, which is held at zero. The rate equations and parameters are as in Ref. 42 (we set the effective extracellular potassium level to 3.5 mM). The values of the external resistive network are all set proportional to the internal dendritic-somatic resistance R^i_{ds} as follows [notation as in Fig. 8(b)]: $R_{ds}=0.1R^i_{ds}$ (note that in the notation of Ref. 42, $R^i_{ds}=1/g\_c$), $R_{td}=R_{sg}=12R_{ds}$, and $R_{dd}=R_{ss}=0.1R_{ds}$. The ends of the resistive network are terminated with finite but smaller resistances designed to approximate an infinitely extending network ($R^{end}_{td}=R^{end}_{sg}=0.5R_{ds}$ and $R^{end}_{ds}=0.145R_{ds}$).

Including the synaptic gating variables, the dynamics of each neuron is modeled by ten coupled first order differential equations. We use a fourth order Runga-Kutta integration scheme, with a fixed time step of 0.05 ms. For a network of ten neurons running on a high end PC, 100 s of integration took of order 50 min.

The dynamics for a network of ten neurons with no applied field is illustrated in Fig. 9. Each trace represents the transmembrane potential at the soma for each neuron (the details of a single neuron firing is in the inset). The population of neurons in the array tends to fire synchronously in bursts. When stimulated at higher extracellular potassium levels, population bursts were more prolonged, with more spikes per neuron during the burst (not shown).

VI. ELECTRIC FIELD INTERACTION

If a time varying electric field is applied to this array, the burst rate is significantly modulated (Fig. 10). In the raster plots of Fig. 10(a), we have plotted a single bar (|) at the spike onset times for each neuron. As the field [Fig. 10(b)], in units [mV/dendrite-soma length], is varied, the interval between network bursts is modulated [Fig. 10(c)], as in the actual experiments (Fig. 4). It has long been known that the magnitude of electric field needed to modulate the firing of a neuron is much smaller than that needed to initiate an action potential from rest,[44] and the physics of this interaction was worked out in detail within the past decade.[45–47] The basic interaction is that ions in both the intracellular and extracellular space move under the influence of the field. However, the ions inside the cells are trapped by the cell membranes, and therefore build up at the ends of the neuron (Fig. 11). If, as in these pyramidal cells, the soma is eccentrically placed with respect to the dendrites, this polarization of the neuron shifts the transmembrane potential at the soma, where action potentials are initiated, with respect to the threshold for ac-

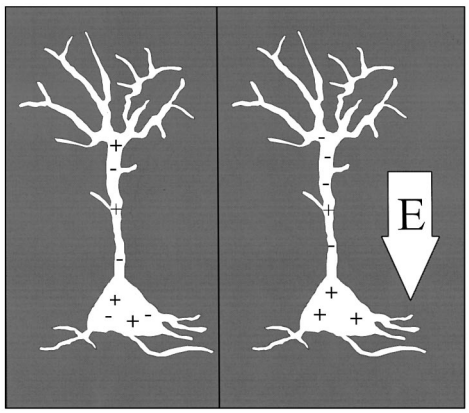

FIG. 11. Idealization of the interaction between the trapped ions in a neuron and an imposed electric field. When a field is applied, the neuron is polarized, shifting the transmembrane potential at the soma, which alters its threshold for action potential initiation.

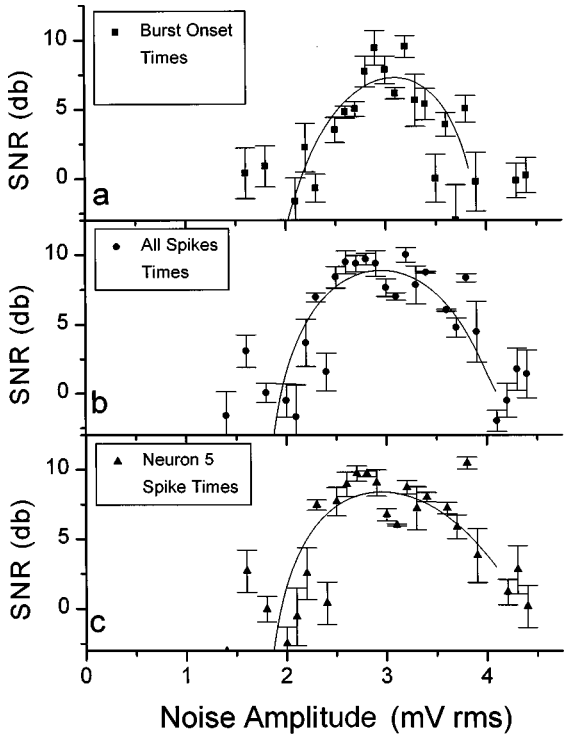

FIG. 12. The SNR as a function of noise amplitude for ten-neuron model network with local coupling ($f_0=0.8$ Hz, $f_N=21.11$ Hz). SNR was computed from the PSD of event times, where events were defined by (a) the network group activity, (b) spike times from each neuron, and (c) spike times from a single neuron in the center of the network. A clear optimization at finite noise level is observed for each case.

tion potential initiation (see Refs. 44–46). Within the hippocampal layers (CA1, CA3, . . .), the pyramidal neurons have long apical dendrites which are aligned approximately parallel to each other, and perpendicular to the layer. Therefore, a field applied perpendicular to the local cell body layer polarizes the population of neurons, on average making them all slightly more or less excitable.

VII. COMPUTATIONAL SR

We were able to demonstrate SR for our computational network of ten neurons in response to an applied field. In order to make the neurons nonbursting with no applied signal, we applied a small bias current to each of the dendrites ($-0.1\ \mu A/cm^2$). Beyond that, all parameters were as before. The sinusoid and noise cutoff frequencies were $f_0=0.8$ Hz and $f_N=21.11$ Hz. The SNR as a function of noise amplitude is shown in Fig. 12. Each data point corresponds to statistics from a 200 s long integration of the model. The different plots refer to different ways of characterizing the observed activity. In Fig. 12(a), the onset times of network bursts were used as the output of the network. In Fig. 12(b), the spike onset times of all of the neurons were used, and in Fig. 12(c), the spike onset times of a single neuron from the center of the network were used. Although there are small differences between these optimization curves, all show an optimization at finite noise amplitude. Similar optimization was observed for a similar integration model with just one neuron and an imposed field (not shown).

VIII. DISCUSSION

We have demonstrated stochastic resonance experimentally in the dynamics of a live neuronal network in response to an applied electric field. These experiments are unique in that electrical fields gave us direct control of both signal and noise across an entire ensemble of neurons, though they are somewhat unrealistic from a computational perspective. Although models of neuronal ensemble SR are typically conceived with independent noise generators for each neuron (e.g., see Ref. 34), using a uniform global noise source in the manner that we have employed here has been well studied theoretically[48] and did not appear to be an impediment to observing SR in our case.

Much controversy has arisen in recent years concerning dynamical versus nondynamical SR.[49,50] Whereas ''classical'' SR was conceptualized as a matching of time scales between noise induced switching of a bistable system with an imposed periodic signal, noise induced optimization of system response was recognized in the simplest of nondynamical threshold systems.[51] The primary dynamical response of a neuron, the firing of an action potential, is excitable rather than bistable (although bistability and even multistability can be seen in more complex neuronal dynamics). However, there is a finite time after excitation during which the neuron repolarizes—the refractory period—within which the threshold for reexcitation is time dependent. The relationship between the period of the stimulation and the refractory period can change the qualitative nature of the observed dynamics.[49,52] When the frequency is high enough that these periods are comparable, dynamical features of SR are observed. On the other hand, when stimulation frequencies are slow compared with the excitation and repolarization of neurons, a more nondynamical picture reminiscent of stochastic linearization or ''dithering''[53] is observed.

In our experiments, we did not record the activity of individual neurons, but rather focused upon an emergent behavior of the neuronal ensemble—population bursts. The characteristic frequencies of these bursts, typically occurring at 0.5–2.0 Hz, was very close to the signal frequencies we employed in order to observe SR ($f_0<4$ Hz). Since the individual neurons tend to fire at higher mean rates than the population bursts, an avenue for future work is to unravel the complex relationships between the individual and ensemble dynamics in systems such as this.

In our preparations, we likely had the interaction of at least four frequencies: the noise induced mean firing rate of the neurons, the sinusoidal electric field, the intrinsic oscillatory frequency of the individual neurons, as well as the intrinsic population burst frequency of the ensemble. In our analysis of these experiments, we could clearly observe the noise optimized presence of our sinusoidal electric field in the output of the neuronal ensembles. Nevertheless, we speculate that a rich set of frequency interactions remains to be uncovered in noise driven ensembles such as this. Although coherence in purely noise driven neuronal models is well described,[54,55] in preliminary experiments with noise driven brain slices we did not observe (unpublished data) phenomena characterized as ''autonomous'' SR.[56]

We generally envision that most information within the central nervous system is carried by action potential spikes. The most direct expression of the SR paradigm would be manifested by a central nervous system that increases the number of random spikes within a neuronal network in order to enhance transmission or information processing, but as of yet of there is no experimental evidence that nervous systems do this.[35] In the experiments studying environmental fluctuations and noise, such as the crayfish mechanoreceptor,[19–21] one can intuitively see the advantages of evolving sensory receptors whose sensitivity peaks with certain levels of environmental noise. Yet away from an organism's sensory system, perhaps central nervous system interneurons have similar detection needs. As highly nonlinear threshold devices, the sensitivity to incoming signals of single neurons and their networked ensembles would be enhanced by a certain level of background activity. Indeed, a characteristic of central nervous system neurons is an incessant and seemingly random level of activity, and multiple spikes need to impinge synaptically on the typical central nervous system neuron in order to gernerate a new spike. In this sense, a certain level of background activity within the central nervous system is likely necessary for optimal signal transmission, and ''noise'' is here any activity unrelated to a given signal of interest. From this perspective, the SR paradigm, enhanced signal response in the presence of uncorrelated activity, may well be widely pervasive within central nervous systems. As multiple processing tasks take place simultaneously within active brains, one neuron's signal may become another neuron's noise.

ACKNOWLEDGMENTS

We would like to acknowledge the participation of E. Neel in these experiments, and helpful discussions with W. L. Ditto, P. Gailey, A. Bulsara, and A. Longtin. This work was supported by the United States National Institutes of Mental Health Grants 1R29-MH50006-04 and 1KO2MH01493-01, the US Department of Energy through subcontract 85X-SX516V with Oak Ridge National Laboratory, the US Office of Naval Research (ONR) Grant N00014-95-1-013 and the ONR Postdoctoral Fellowship Program, and The Children's Research Institute.

[1] W. R. Adey, ''Organization of brain tissue: Is the brain a noisy processor?'' Intern. J. Neuroscience **3**, 271–284 (1972).
[2] F. Moss and K. Wiesenfeld, ''The Benefits of Background Noise,'' Sci. Am. **2**, 68–77 (1995).
[3] K. Wiesenfeld and F. Moss, ''Stochastic resonance and the benefits of noise: from ice ages to crayfish and SQUIDs,'' Nature (London) **373**, 33–36 (1995).
[4] A. Bulsara and L. Gammaitoni, ''Tuning in to Noise,'' Phys. Today **49**, 39–45 (1996).
[5] A. Longtin, A. Bulsara, and F. Moss, ''Time-interval sequences in bistable systems and the noise-induced transmission of information by sensory neurons,'' Phys. Rev. Lett. **67**, 656–659 (1991).
[6] D. R. Chialvo and A. V. Apkarian, ''Modulated Noisy Biological Dynamics: Three Examples,'' J. Stat. Phys. **70**, 375–391 (1993).
[7] S. M. Bezrukov and I. Vodyanoy, ''Noise induced enhancement of signal transduction across voltage-dependent ion channels,'' Nature (London) **378**, 362–364 (1995).
[8] S. M. Bezrukov and I. Vodyanoy, ''Stochastic resonance in noncdynamical systems without response thresholds,'' Nature (London) **385**, 319–321 (1997).
[9] P. C. Gailey, A. Neiman, J. J. Collins, and F. Moss, ''Stochastic Resonance in Ensembles of Nondynamical Elements: The Role of Internal Noise,'' Phys. Rev. Lett. **79**, 4701–4704 (1997).
[10] A. Bulsara, E. W. Jacobs, T. Zhou, F. Moss, and L. Kiss, ''Stochastic resonance in a single neuron model: Theory and analog simulation,'' J. Theor. Biol. **52**, 531–555 (1991).
[11] A. Longin, ''Stochastic resonance in neuronal models,'' J. Stat. Phys. **70**, 309–327 (1993).
[12] K. Wiesenfeld, D. Pierson, E. Pantazelou, C. Dames, and F. Moss, ''Stochastic Resonance on a Circle,'' Phys. Rev. Lett. **72**, 2125–2129 (1994).
[13] A. R. Bulsara, S. B. Lowen, and C. D. Rees, ''Cooperative behavior in the periodically modulated Wiener process: Noise-induced complexity in a model neuron,'' Phys. Rev. E **49**, 4989–5000 (1994).
[14] P. Jung, ''Threshold devices: Fractal noise and neural talk,'' Phys. Rev. E **50**, 2513–2522 (1994).
[15] M. Riani and E. Simonotto, ''Stochastic resonance in the perceptual interpretation of ambiguous figures: a neural network model,'' Phys. Rev. Lett. **72**, 3120–3123 (1994).
[16] J. J. Collins, C. C. Chow, and T. T. Imhoff, ''Stochastic resonance without tuning,'' Nature (London) **376**, 236–238 (1995).
[17] P. Jung and G. Mayer-Kress, ''Spatiotemporal stochastic resonance in excitable media,'' Phys. Rev. Lett. **74**, 2130–2133 (1995).
[18] X. Pei, L. Wilkens, and F. Moss, ''Noise-mediated spike timing precision from aperiodic stimuli in an array of Hodgekin-Huxlely-Type neurons,'' Phys. Rev. Lett. **77**, 4679–4682 (1996).
[19] J. K. Douglass, L. Wilkens, E. Pantazelou, and F. Moss, ''Noise enhancement of information transfer in crayfish mechanoreceptors by stochastic resonance,'' Nature (London) **365**, 337–340 (1993).
[20] E. Pantazelou, C. Dames, F. Moss, J. Douglass, and L. Wilkens, ''Temperature dependence and the role of internal noise in signal transduction efficiency of crayfish mechanoreceptors,'' Int. J. Bifurcation Chaos Appl. Sci. Eng. **5**, 101–108 (1995).
[21] X. Pei, L. A. Wilkens, and F. Moss, ''Light enhances hydrodynamic signaling in the multimodal caudal photoreceptor interneurons of the crayfish,'' J. Neurophysiol. **76**, 3002–3011 (1996).
[22] J. E. Levin and J. P. Miller, ''Broadband neural encoding in the cricket cercal sensory system enhanced by stochastic resonance,'' Nature (London) **380**, 165–168 (1996).
[23] J. J. Collins, T. T. Imhoff, and P. Grigg, ''Noise-enhanced Information transmission in rat SA1 cutaneous mechanoreceptors via aperiodic stochastic resonance,'' J. Neurophysiol. **76**, 642–645 (1996).
[24] P. Cordo, J. T. Inglis, S. Verschueren, J. J. Collins, D. M. Merfeld, S. Rosenblum, S. Buckley, and F. Moss, ''Noise in human spindles,'' Nature (London) **383**, 769–770 (1996).
[25] J. J. Collins, T. T. Imhoff, and P. Grigg, ''Noise-enhanced tactile sensation,'' Nature (London) **383**, 770 (1996).
[26] E. Simonotto, M. Riani, C. Seife, M. Roberts, J. Twitty, and F. Moss, ''Visual Perception of Stochastic Resonance,'' Phys. Rev. Lett. **78**, 1186–1189 (1997).
[27] B. J. Gluckman, T. I. Netoff, E. J. Neel, W. L. Ditto, M. L. Spano, and S. J. Schiff, ''Stochastic Resonance in a Neuronal Network from Mammalian Brain,'' Phys. Rev. Lett. **77**, 4098–4101 (1996).
[28] B. J. Gluckman, E. J. Neel, T. I. Netoff, W. L. Ditto, M. L. Spano, and S. J. Schiff, ''Electric field suppression of epileptiform activity in hippocampal slices,'' J. Neurophysiol. **76**, 4202–4205 (1996).
[29] R. Benzi, A. Sutera, and A. Vulpiani, ''The mechanism of stochastic resonance,'' J. Phys. A **14**, L453–L457 (1981); R. Benzi, G. Parisi, A. Sutera, and A. Vulpiani, ''Stochastic resonance in climatic change,'' Tellus **34**, 10–16 (1982).
[30] L. Gammaitoni, F. Marchesoni, and S. Santucci, ''Stochastic resonance as a *Bona Fide* resonance,'' Phys. Rev. Lett. **74**, 1052–1055 (1995).
[31] J. J. Collins, C. C. Chow, A. C. Capela, and T. I. Imhoff, ''Aperiodic stochastic resonance,'' Phys. Rev. E **54**, 5575–5584 (1996).
[32] C. Heneghan, C. C. Chow, J. J. Collins, T. T. Imhoff, S. B. Lowen, and M. C. Teich, ''Information measures quantifying aperiodic stochastic resonance,'' Phys. Rev. E **54**, R2228–R2231 (1996).
[33] C. Eichwald and J. Walleczek, ''Aperiodic stochastic resonance with chaotic input signals in excitable systems,'' Phys. Rev. E **55**, R6315–R6318 (1997).
[34] J. J. Collins, C. C. Chow, and T. T. Imhoff, ''Stochastic resonance without tuning,'' Nature (London) **376**, 236–238 (1995).
[35] M. Stemmler, ''A Single Spike Suffices: The Simplest Form of Stochastic

Resonance in Model Neurons,'' Network: Computation in Neural Systems **7**, 687–716 (1996).
[36] A. Neiman, B. Shulgin, V. Anishchenko, W. Ebeling, L. Schimansky-Geier, and J. Freund, ''Dynamical Entropies Applied to Stochastic Resonance,'' Phys. Rev. Lett. **76**, 4299–4302 (1996).
[37] For anatomy, see A. Brodal, *Neurological Anatomy, Third Edition* (Oxford U. P., New York, 1981).
[38] W. H. Press, S. A. Teukolsky, W. T. Vetterling, and B. P. Flannery, *Numerical Recipes in C, The Art of Scientific Computing, Second Edition* (Cambridge U. P., Cambridge, 1992), p. 550.
[39] H. C. Tuckwell, *Introduction to Theoretical Neurobiology* (Cambridge U. P., Cambridge, 1988), Vol. 2.
[40] T. E. Holy, ''Analysis of Data from Continuous Probability Distributions,'' Phys. Rev. Lett. **79**, 3545–3548 (1997).
[41] T. Zhou, F. Moss, and P. Jung, ''Escape-time distributions of a periodically modulated bistable system with noise,'' Phys. Rev. A **42**, 3161–3169 (1990).
[42] P. F. Pinsky and J. Rinzel, ''Intrinsic and Network Rhythmogenesis in a Reduced Traub Model for CA3 neurons,'' J. Computational Neuroscience **1**, 39–60 (1994).
[43] R. Traub, R. Miles, and G. Buzsaki, ''Computer simulation of carbochol-driven rhythmic population oscillations in the CA3 region of the in vitro rat hippocampus,'' J. Physiol. (London) **451**, 653–672 (1991).
[44] J. G. R. Jefferys, ''Influence of electric fields on the excitability of granule cells in guinea-pig hippocampal slices,'' J. Physiol. (London) **319**, 143–152 (1981).
[45] C. Y. Chan and C. Nicholson, ''Modulation by applied electric fields of Purkinje and stellate cell activity in the isolated turtle cerebellum,'' J. Physiol. (London) **371**, 89–114 (1986).
[46] C. Y. Chan, J. Houndsgaard, and C. Nicholson, ''Effects of electric fields on transmembrane potential and excitability of turtle cerebellar Purkinje cells *in vitro*,'' J. Physiol. (London) **402**, 751–771 (1988).
[47] D. Tranchina and C. Nicholson, ''A model for the polarization of neurons by extrinsically applied electric fields,'' Biophys. J. **50**, 1139–1159 (1986).
[48] M. E. Inchiosa and A. R. Bulsara, ''Nonlinear dynamic elements with noisy sinusoidal forcing: Enhancing response via nonlinear coupling,'' Phys. Rev. E **52**, 327–339 (1995).
[49] D. R. Chialvo, A. Longtin, and J. Muller-Gerking, ''Stochastic resonance in models of neuronal ensembles,'' Phys. Rev. E **55**, 1798–1808 (1997).
[50] F. Chapeau-Blondeau and X. Godivier, ''Theory of stochastic resonance in signal transmission by static nonlinear systems,'' Phys. Rev. E **55**, 1478–1495 (1997).
[51] F. Chapeau-Blondeau, ''Stochastic resonance in the heavyside nonlinearity with white noise and arbitrary periodic signals,'' Phys. Rev. E **53**, 5469–5472 (1996).
[52] A. Longtin and D. R. Chialvo, ''Stochastic and deterministic resonances (Arnold tongues) for excitable systems,'' (to appear).
[53] L. Gammaitoni, ''Stochastic resonance and the dithering effect in threshold physical systems,'' Phys. Rev. E **52**, 4691–4698 (1995).
[54] W.-J. Rappel and A. Karma, ''Noise-induced coherence in neural networks,'' Phys. Rev. Lett. **77**, 3256–3259 (1996).
[55] A. S. Pikovsky and J. Kurths, ''Coherence resonance in a noise-driven excitable system,'' Phys. Rev. Lett. **78**, 775–778 (1997).
[56] A. Longtin, ''Autonomous stochastic resonance in bursting neurons,'' Phys. Rev. E **55**, 868–876 (1997).